Distributed X-ray dosimetry with optical fibers by Optical Frequency Domain Interferometry

Distributed X-ray dosimetry with optical fibers by Optical Frequency Domain Interferometry

Massimo Olivero, Alessandro Mirigaldi,Valentina Serafini, Alberto Vallan, Guido Perrone, *DET*
Politecnico di Torino
Torino, Italy
Wilfried Blanc, Mourad Benabdesselam, Franck Mady *Université Côte d'Azur, CNRS*
INPHYNI, UMR 7010
Nice, France
Carlo Molardi, Daniele Tosi *School of Engineering and Digital Sciences*
Nazarbayev University
Nur-Sultan, Kazakhstan

***Abstract*—The paper reports on the first demonstration of in-situ, real-time dosimetry realized with an enhanced back-scattering optical fiber and a high-resolution optical back-scattering reflectometry measurement. This work is devised to overcome the current problems in monitoring radiotherapy treatments, in particular the difficult evaluation of not only the actual X-ray dose that is accumulated on the target volume, but also the distribution profile of the ionizing radiation beam. Overall, the research aims at developing a dose sensor with the most demanding features of small form factor, spatial profiling and remote interrogation. The experiments have been conducted by evaluating the spatial profile of radiation-induced spectral shift of the Rayleigh back-scattering along an optical fiber exposed to X-rays. The sensing element is a section of specialty optical fiber whose Rayleigh back-scattering signature changes under ionizing radiation. The specialty fiber is designed to exhibit an enhanced back-scattering, in order to overcome the poor sensitivity to radiation of standard optical fibers that are normally used in telecommunications. The enhanced sensitivity is achieved by doping of the core with either Aluminum or Magnesium nanoparticles and two different fibers have been fabricated and tested. The experimental results show the capability of real time detection of the radiation profile from high dose rates ($700\,\mathrm{Gy/min}$) to low dose rates ($2\,\mathrm{Gy/min}$). Moreover, different sensing mechanisms and responses to high and low dose rates are evidenced. A comparison with a quasi-distributed sensing system based on an array of fiber Bragg gratings is discussed, highlighting the superior performance of the back-scattering approach in terms of sensitivity and spatial resolution, whereas the array of fiber Bragg gratings exhibits an advantage in terms of sampling speed.**

***Index Terms*—Optical fiber sensors, Radiation monitoring, Radiation dosage, Ionizing radiation sensors**

I. Introduction

Ionizing radiations find many medical applications, going from diagnostic, such as in Computed Tomography (CT), to therapeutics, such as in tumor radiotherapy. These two fields are characterized by quite different dose levels, practically at the opposite of the scale: extremely low doses for imaging to investigate tissues without producing damages and relatively high doses for radiotherapy to kill cancer cells or slows their growth by damaging their DNA. In both cases, however, modern medical protocols require accurate monitoring of the dose at which the patient is exposed. While this can be straightforward to understand for the high-doses used in therapeutic applications, it has to be pointed out that low doses used in imaging equipment can be harmful too; for example, if for some reason the instrument stops working properly: the literature reports cases of patients who have filed lawsuits for having suffered burns from extreme over-exposures during CT exams, due to improper settings on the CT scanners.

Ionizing radiations can be measured using a number of instruments, the most common being personal dosimeters in the form of film badges worn on clothing, which measure the cumulative radiation dose a person receives while exposed to radiation sources. More quantitative evaluations can be made with hand-held detectors, such as Geiger-Müller counters and ionization chambers, which are used to measure the exposure rate from a source (for example, emissions from radioactive wastes). In medical applications, however, it is interesting not only to measure the total dose at which the patient is exposed, but also the spatial distribution of the radiation in the target volume. Unfortunately, the latter measurement is difficult to implement in real time before and during the treatment. Indeed, the previously mentioned radiation monitoring instruments cannot be used because they measure the amount of radiation on a quite large area and thus are not easy to be multiplexed to recover the radiation distribution, not to mention the poor resolution achievable in that case. The most common technique to evaluate the intensity distribution is to use GafChromic (GaF) films. These films contain a special dye that polymerizes upon exposure to radiation, with a subsequent increase in its absorption at optical frequencies; that is, the optical density (OD) of the film increases with the dose [1], turning it more opaque (Fig. 1).

Another alternative proposed in the literature exploits gel-based nano-sensors in which exposure to ionizing radiation results in the conversion of gold ions to nanoparticles, with subsequent visual change in color due to their plasmonic properties [2]. Both approaches, however, cannot be used for real-time continuous measurements [3].

Optical fibers can constitute an attractive alternative technology for the realization of a new class of ionizing radiation

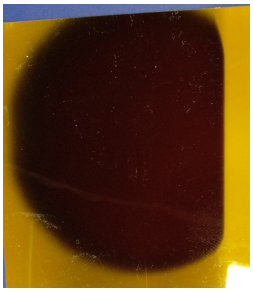

Fig. 1. GaF film exposed at 700 Gy/min. The spot size is about 20 mm .

sensors thanks to a number of unique features, among which: i) they are minimally invasive; ii) can be remotely interrogated; iii) do not involve electrical currents (a plus feature in medical applications as it intrinsically avoids electrocution). Standard optical fibers for telecommunication applications are made by ultra-pure silica, with some dopants added to slightly increase the refractive index in the core region (usually, Germanium or Phosphorus), and exhibit little sensitivity to ionizing radiations; however, it is know from literature that this low sensitivity can be enhanced by co-doping with Aluminum.

The sensitivity of fibers to radiation typically manifests in the form of Radiation Induced Attenuation (RIA), for which the propagation loss of an irradiated fiber is higher than that of the pristine fiber. This is a local effect, so the loss increase against the fiber length is proportional to the cumulative radiation along the fiber. In other words, this effect can be exploited to evaluate the radiation intensity profile by measuring the loss spatial distribution along the fiber, a kind of measurement that in telecommunication applications is performed with an Optical Time Domain Reflectometer (OTDR). In the OTDRs a light pulse of known width is transmitted through the fiber and the reflected power and the time of flight are measured to determine the magnitude and location of the perturbations along the fiber. An application of OTDRs for long-range gamma-ray detection has been presented in [4]. Furthermore, the OTDR technique has been used to qualify the RIA of different optical fibers, by exposing samples of lengths about 10 m [5]. However, besides for having a dead zone (i.e., an initial length in which the interrogator is blind) in the order of meters, OTDRs are non suitable for radiotherapy dosimetry applications for the poor resolution, in terms of both loss and position, especially considering that for this application the radiation intensity (and thus the loss variation) is expected to be small and the dose profile should ideally be measured with sub-cm resolution. Therefore, another radiation-dependent feature must be investigated. When an optical signal propagates along a fiber, a small amount of its power is back-scattered because of a phenomenon known as the Rayleigh scattering, which depends on the local composition fluctuation in a sub-wavelength scale. The associated attenuation is usually low in commercial fibers and, as previously stated, quite insensitive to radiation. On the other hand, the real part of the refractive index, responsible for the phase delay of signal propagating along the fiber, Can be more effectively correlated to ionizing radiation. In particular, the Rayleigh back-scattering can be measured with high accuracy through Optical Frequency Domain Reflectometry (OFDR). The principle of operation of OFDR may be better explained with the help of the schematic in Fig. 2. OFDR instruments rely on a swept wavelength laser coupled into a modified Mach-Zender interferometer. One leg of the interferometer is a reference path of fixed length, while the other leg is the optical fiber under test interrogated in reflection through a directional coupler. The backscattered light is combined with the light from the reference arm generating an interference signal that contains information related to the accurate location (i.e. with sub mm resolution) and magnitude of reflective events along the fiber length. Actually, an acquisition system collects a large number of intensity signals from the detector, as a function of wavelength and time (by performing multiple sweeps). The intensity patterns are cross correlated and from the cross-correlation function (or better, its Fourier transform) it is possible to retrieve the complete spectral response (both in terms of real and imaginary parts) at any position along the fiber under test. Thus, the OFDR is able to measure the precise location of very small reflective events with no dead zone.

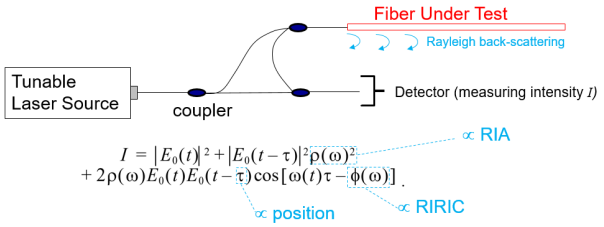

Fig. 2. Schematic representation of the OFDR principle of operation. The intensity I measured by the detector contains information about the Radiation-Induced Refractive Index Change (RIRIC) and the Radiation-Induced Attenuation (RIA) along the fiber under test. $|E_0(t)|^2$ is the intensity provided by the tunable laser and $\rho(\omega)$ the spectral response of the device (in this case a fiber) under test; ω is related to the current wavelength of the swept laser and t and τ are the time and time delay of the observation. By performing autocorrelation and subsequent Fourier transform of I it is possible to evaluate RIA and RIRIC along the fiber.

A recent review article, with details on the principle of operation as well as a comprehensive overview of its sensing applications can be found in [6]

In this work, Enhanced Backscattering optical Fibers (EBFs) were exposed to X-rays while their Rayleigh scattering was recorded using an OFDR. Then the Rayleigh scattering signature was processed in real time to calculate a spectral shift parameter that could be correlated to the dose, through a linear relationship. The radiation induced attenuation was also measured to prove its weak effect and the need of more advanced measurement techniques such as the OFDR for the evaluation of the radiation profile. The novelty of this research relies both in exploiting radiation-sensitive custom-made optical fibers and in investigating the spectral shift of the Rayleigh backscattering rather than measuring the RIA, by exploiting a high resolution OFDR interrogation. The results are expected to pave the way to the development of novel distributed dosimeters based on optical fibers. The work here

reported is an extension of that presented at the 15th Edition of IEEE International Symposium on Medical Measurements and Applications (MeMeA 2020) [7] and it reports a remarkable amount of new analyses, extending the scope of the former manuscript to the comparison of two different enhanced backscattering optical fibers while reporting a considerable improvement in data acquisition reliability. Last but not least, the current work also reports the response to X-ray exposure of femtosecond-written fiber Bragg gratings (FBGs) in one of the enhanced backscattering fibers, confirming the capability to measure the RIRIC along the irradiated fiber and opening an alternative for quasi-distributed radiation profile evaluation.

II. Measurement Setup

The experimental setup is sketched in Fig. 3 and it is build around an interrogation unit constituted by a Luna OBR4600 Optical Backscatter Reflectometer (OBR) [8]. The OBR is a swept-laser interferometer that implements an optical frequency-domain reflectometry (OFDR) principle. The system is capable of sensing Rayleigh scattering signatures along the fiber under test, with a nominal spatial resolution of $< 10\,\mu\mathrm{m}$, operating on a $88\,\mathrm{nm}$ wavelength grid centered around the infrared C-band ($1550\,\mathrm{nm}$) [9], [10]. The fiber to be tested as a dosimeter is positioned in a shielded radiation chamber, under an X-ray beam, and connected to the OBR through an about $4.5\,\mathrm{m}$ standard Single Mode Fiber (SMF). The X-ray generator (INEL, model XRG3D) is based on a tube containing a copper target with an accelerating voltage of $30\,\mathrm{kV}$. The cone-like X-ray emission, produced in air and at room temperature, is controlled by adjusting the supplied electrical current and the distance between the generator and the fiber under test. The beam was calibrated, in terms of dose rate, by means of a flat ionization chamber (PTW, model 23342) and a high precision/high resolution electrometer (PTW, model UNIdos E).

Three different irradiation conditions were considered: i) a very high dose by positioning the fiber $26\,\mathrm{mm}$ from the source window, leading to a dose rate of about $710\,\mathrm{Gy/min}$; ii) a medium-high dose obtained by moving the fiber down to $295\,\mathrm{mm}$ from the source window, corresponding to a lower dose rate of about $22\,\mathrm{Gy/min}$; iii) a low-dose of about $2\,\mathrm{Gy/min}$ resulting from positioning the fiber about $70\,\mathrm{mm}$ from the source.

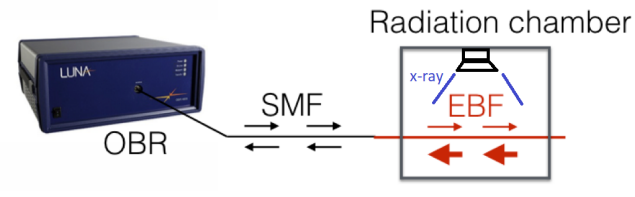

Fig. 3. Schematic representation of the measurement setup.

To overcome the known poor sensitivity to radiation of standard SMFs used in telecommunications (a feature appreciated for that application), the sensing section is an alumino-silicate fiber that exhibits enhanced backscattering. For some of the experiments a further improved nanoparticles-doped version was used, in which the core is doped with Magnesium-based (Mg) nanoparticles, hereby denoted as NPEBF. The fabrication process of these fibers is detailed in several publications, such as in Ref. [11], [14]. It it consists of a preform fabrication by a standard Modified Chemical Vapor Deposition (MCVD) technique followed by fiber drawing, in which a silicate tube is used to build the preform. The core layers are deposited at a reduced temperature so as to form an unsintered porous soot. The solution doping technique [12] is applied to incorporate Al or Mg ions in the core. For this step, the tube is subsequently removed from the lathe and soaked in a alcoholic solution containing the dopant precursor of desired concentration. After drying of the solvent, the tube is replaced in the lathe and heated to produce sintering of the core into a dense glass layer. Finally, it is collapsed at an elevated temperature, higher than $1800\,^{\circ}\mathrm{C}$, into a solid rod that constitutes the preform for optical fiber drawing. Mg-based nanoparticles in the NPEBF preform are formed due to the phase separation occurring at high temperature [21]. The preform is pulled at high temperature ($>2000\,^{\circ}\mathrm{C}$) into a drawing tower to produce an optical fiber with core/cladding diameter of $10/125\,\mu\mathrm{m}$, respectively. SMF and EBF fibers are spliced with a standard fusion splicer, as they have matching core/cladding sizes and similar effective refractive index.

The former experiments presented in the previous MeMeA paper were taken by manually recording the Rayleigh signatures at a rate of about 1 acquisition/min and the exposures lasted $10\,\mathrm{min}$. The setup has been then upgraded by implementing an automatic acquisition system. To do so, the Luna OBR4600 is controlled through a custom Labview™ program that implements a handshaking between the controlling computer and the instrument. This way, the acquisition rate is pushed to the instrument capability, which depends on the measurement parameters. The results presented in the following were obtained by setting a spatial resolution of $0.1\,\mathrm{mm}$ and a gage length of $10\,\mathrm{to}\,30\,\mathrm{mm}$, which allowed for the acquisition of one spatial signature every $30\,\mathrm{s}$. The gage length represents an equivalent sensor length (or, in other words, the number of points) on which the Rayleigh backscattering parameters are computed. Faster recordings could be possible by setting higher (i.e. poorer) spatial resolutions and/or higher gage lengths, but it must be pointed out that, in any case, the heavy data processing burden limits the capability of the instruments to acquisitions rates in the order of seconds.

III. Experimental Results

A. Assessment of the enhanced-backscattering fiber

The effects of exposure to X-rays was evaluated in terms of the spectral shift of the Rayleigh scattering signature versus longitudinal position along the EBF. In order to qualitatively understand the rationale of spectral shift, one can consider the exposed fiber as a cascade of densely spaced weak Fiber Bragg Gratings (FBGs) [15]. These FBG back-scatter a portion of the signal provided by the swept laser of the OBR instruments, thus producing a reference signature of that fiber (the Rayleigh-scattering signature). Any change in the refractive

index or in the pitch of each grating will produce a spectral shift of its Bragg reflection peak; the collection of these shifts represents the spectral shift curve with respect to the pristine fiber signature. The procedure to measure the spectral shift along the fiber is then performed in a two-steps process: the reference signature is acquired in steady conditions, first; then Rayleigh back-scattering spectra are subsequently recorded and cross correlated to the reference to retrieve the spectral shift (these operations are performed by the OBR instrument).

The fiber under exposure was firmly fixed and kept at constant temperature, so that the spectral shift could only be ascribed to the effect of radiation. As already mentioned, the OBR was computer-controlled through a custom developed program that recorded the spectral shift every $30\,\mathrm{s}$, with a spatial resolution set to $5\,\mathrm{mm}$.

As a preliminary test, a high dose rate of $700\,\mathrm{Gy/min}$ was used; the resulting spectral shift is reported in Fig. 4. The graph demonstrates that the considered fiber is sensitive to such high dose because a clear strong modification of the spectral shift appears exactly where the X-ray exposure occurred. Moreover, the Full Width Half Minimum (FWHM) of the dip is about $20\,\mathrm{mm}$, in good agreement with a comparative measure performed by GaF films.

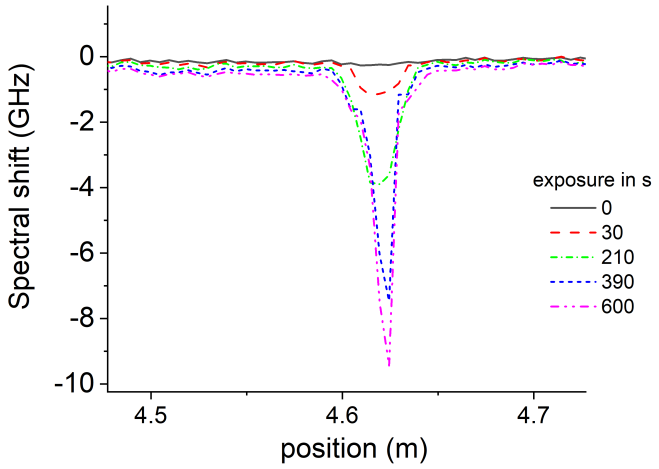

Fig. 4. Spectral shift versus position along the EBF for different exposure times at $700\,\mathrm{Gy/min}$. The spatial resolution of the data is $5\,\mathrm{mm}$.

A negative spectral shift is induced, producing a dip that deepens as the energy is deposited on the fiber. Once the X-ray beam is turned off, a partial recovery of the spectral shift is observed, indicating a possible reversible process (permanent-induced defects are likely to occur at higher doses, as observed for example by Girard *et. al* [16]). The dynamics of the dip at the position $4.62\,\mathrm{m}$, observable in Fig. 5, is reasonably well approximated by a linear dependence on the dose during the exposure. The recovery, instead, exhibits a more complex trend, but in the graph it is linearly fitted to highlight the change of sign in the slope and to give a rough estimation of the recovery time, that is about $0.73\,\mathrm{GHz/min}$.

In order to make a quantitative comparison of the sensitivity of the EBF with a standard SMF, the same experiment at

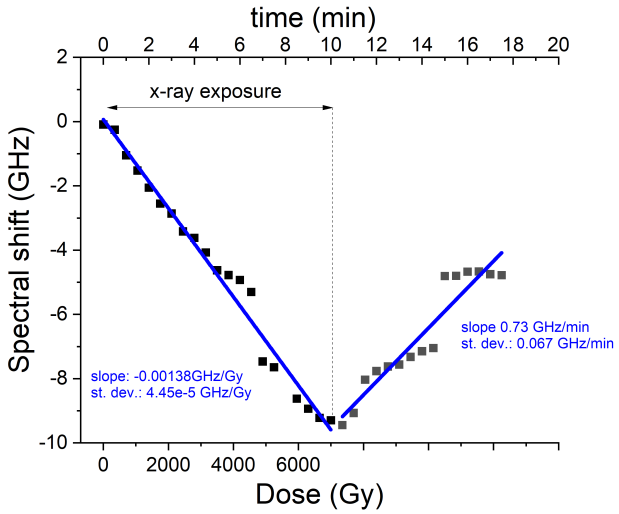

Fig. 5. Spectral shift versus exposure time and corresponding dose for the EBF at $700\,\mathrm{Gy/min}$.

the high dose rate of $700\,\mathrm{Gy/min}$ was repeated exposing an SMF pigtail (G652 compatible fiber). The SMF exhibited, as expected, a much smaller, yet still detectable, spectral shift located at the exposed section, as shown in Fig. 6.

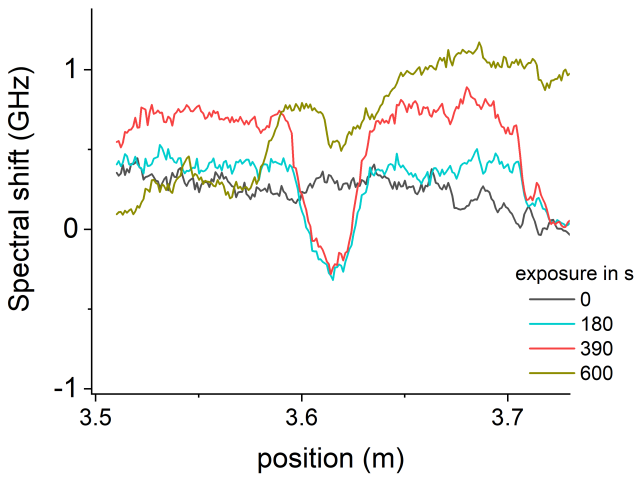

Fig. 6. Spectral shift versus position for a standard SMF (G652 compliant fiber) exposed at $700\,\mathrm{Gy/min}$.

The final spectral shift for a cumulative dose of $5200\,\mathrm{Gy}$ was about $0.3\,\mathrm{GHz}$ and did not show any further change with time. Fig. 7 reports the spectral shift evolution versus time and corresponding dose. The graph axes are set on the same scales as Fig. 5 to make a straightforward comparison and highlight the different sensitivities between the EBF and the SMF.

The Al-doped fiber was also tested at low dose of $22\,\mathrm{Gy/min}$ (Fig. 8), exhibiting a similar trend for the accumulated dose as for the high-dose exposure (Fig. 9). In both high- and low-dose experiments, the linear dependence between spectral shift and dose exhibits a slope in the order of magnitude of 0.001-$0.002\,\mathrm{GHz/Gy}$.

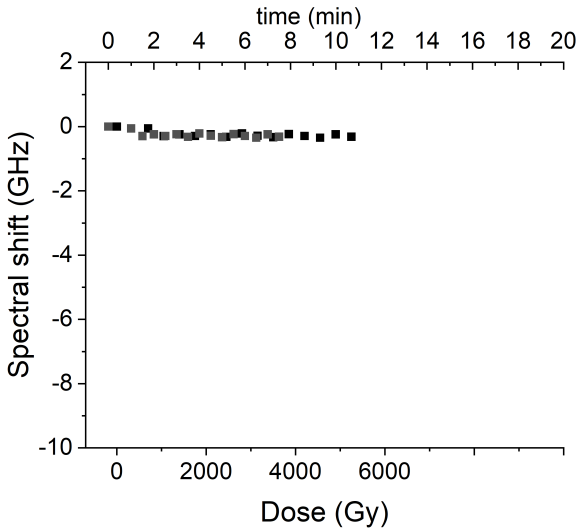

Fig. 7. Evolution of the spectral shift for an SMF exposed at 700 Gy/min.

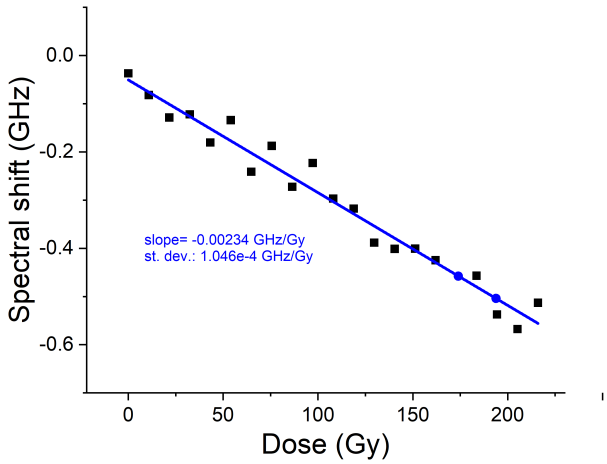

Fig. 9. Spectral shift versus accumulated dose at 22 Gy/min for the EBF.

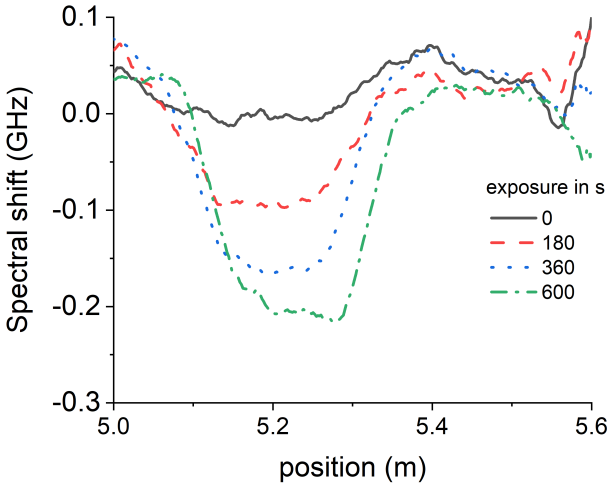

Fig. 8. Spectral shift versus position along the EBR fiber for different times of exposure at 22 Gy/min.

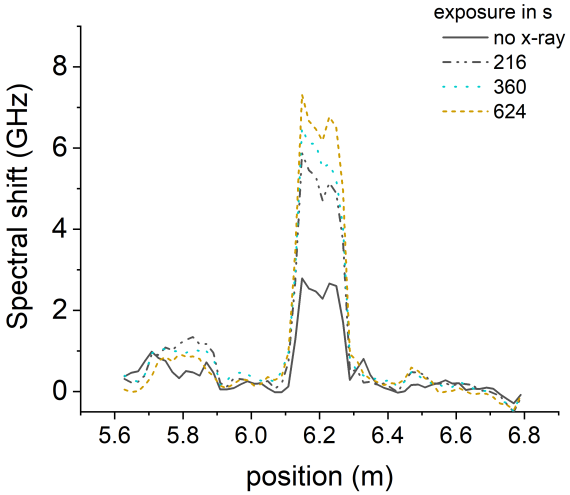

Fig. 10. Spectral shift versus position along the fiber for different times of exposure at 2 Gy/min.

It must be pointed out that the fairly poor reproducibility of the slope coefficient can be ascribed to two reasons: i) the recordings at 22 Gy/min were performed with slightly different settings of the OBR to enhance the sensitivity; and ii) still the data from the experiment at 22 Gy/min were at the limit of sensitivity of the instrument and had to be smoothed by adjacent averaging for representation in Fig. 8 and Fig. 9). Therefore the actual relationship between spectral shift and dose for the considered fiber will have to be further investigated by repeated measurements.

In a third set of experiments, the Al-doped fiber was also tested at even lower dose rate of 2 Gy/min, considering that a total dose of 2 Gy is a reference value for a single session of conventional radiotherapy treatment. The interesting outcome of these measurements is summarized in Fig. 10 and Fig. 11.

The first observation is that the spectral shift, thus the correspondent refractive index change, has opposite sign with respect to the case of higher doses. This confirms a qualitative observation that was also made during high dose exposures that is, the spectral shift of the irradiated region of the fiber seemed to grow and then quickly drops to negative values as the dose accumulates (notice that the the data recording rate of 1 profile/30 s, limited by the instrument's settings of gauge resolution and measurement length, does not allow to clearly report the phenomenon on the graphs). This suggests that there are different competing mechanisms of radiation-induced defects, one prevailing for low doses, but then quickly overcome as the dose increases. Fig. 11 shows a detectable growth with a non-linear trend of the spectral shift and no bleaching effect. Instead, when the X-ray exposure is turned off, a smooth growth seems to occur, but this is likely to be an artifact since all the data are within the measurement noise as evident from the error bars. The height of the error bars is calculated as the standard deviation of the noise floor of all

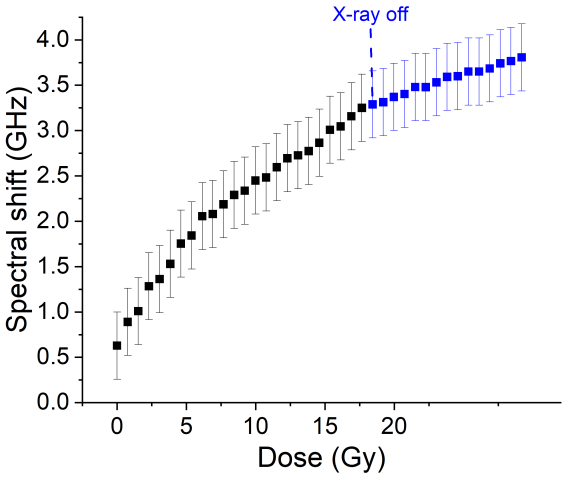

Fig. 11. Spectral shift versus accumulated dose at $2\,\mathrm{Gy/min}$.

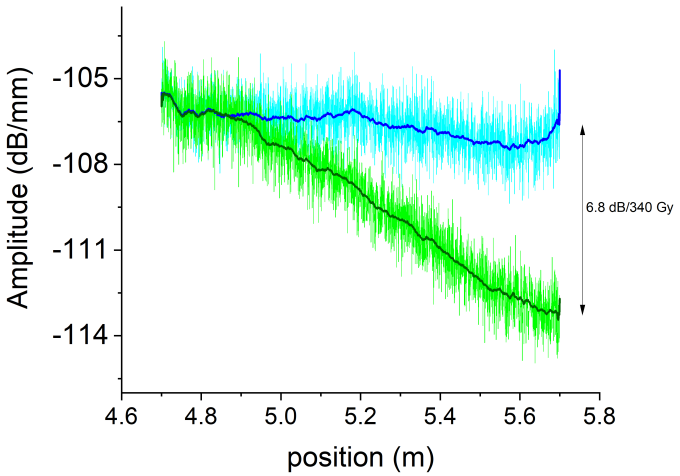

Fig. 12. Rayleigh back-scattering signatures of a $1\,\mathrm{m}$-long coiled fiber, as pristine (cyan curve) and after exposure at $22\,\mathrm{Gy/min}$. A RIA of $6.8\,\mathrm{dB}$ can be observed.

collected spectra shift spatial distributions (notice that Fig. 10 only reports few of the collected curves). The error bars are here reported to highlight that the low dose measurement is affected by non-negligible noise fluctuations that may also ascribed to the close position of the OBR instrument to the radiation chamber.

Finally, the previous graphs demonstrate, as a proof-of-concept, that the alumino-silicate fibers can be used as a distributed dosimeter by measuring the radiation-induced spectral shift with an OBR. Although the idea of using an EBF and an OBR for distributed sensing in therapeutic applications has previously been conceived [17] for measurement of the spatial distribution of temperature, this work represents the first demonstration of real-time in-situ monitoring of radiation with an EBF and OBR technique.

The previous graphs also highlight that the spectral shift is a relevant parameter to track the dose evolution in time. On the other hand, fairly simple measurement of radiation-induced attenuation, which could be performed with a cost-effective OTDR, has been proved not to be effective. Indeed, during the previous experiments, the RIA was also measured by the OBR, but negligible values were recorded. In particular, in order to verify whether a weak RIA occurred, a $1\,\mathrm{m}$-long coiled fiber was exposed at $22\,\mathrm{Gy/min}$ for at $10\,\mathrm{min}$. Fig. 12 reports the outcome of this test and shows a RIA of 6.8 dB, meaning about 0.07 dB over $10\,\mathrm{mm}$. Such a low value is close to the amplitude resolution limit of an OTDR (0.01 dB). Together with its limited spatial resolution (about $10\,\mathrm{mm}$), OTDR seems therefore not as suitable as OBR for optical fiber dosimetry.

Further investigations were then performed in order to assess the potential use of the OBR/EBF system in X-ray dosimetry. From an application viewpoint, it must be pointed out that conventional radiotherapy treatments are performed with a dose of about $2\,\mathrm{Gy/day}$ on a 5-day treatment and the standard dose rate is about $0.2\,\mathrm{Gy/min}$. With these values, The OBR/EBF system is borderline in terms of sensitivity. Therefore, new fibers with further enhanced backscattering capabilities will have to be developed to be employed for such applications. On the other hand, new radio-therapeutic techniques, such as flash radiotherapy (Flash-RT) and stereotactic body radiotherapy (SBRT), exploit much higher dose rates and hence matching the sensitivity of the proposed system [18] [19] [20], which, however, requires certain measurement cares to provide meaningful results. Therefore, the possibility to use more consolidated optical sensing approaches, such as those based on fiber Bragg gratings, would certainly help the wide deployment of these new fiber-based dosimeters. Besides, such an approach allows also overcoming the acquisition rate limitations intrinsic to the OBR approach, thus making the measure "more real-time".

Following these considerations, the experimental research was then focused on two tasks: i) exploring the possibility of tailoring the characteristics of the sensing fiber by proper doping of the core to enhance the sensitivity; ii) make a real-time comparison between the OBR/EBF that works as a fully distributed sensing system and a conventional optical fiber quasi-distributed measurement, realized with an array of fiber Bragg gratings (FBGs) interrogated with a standard high speed FBG interrogator.

B. Nano-particle doped EBF

The first task was implemented by testing the a Magnesium-based (Mg) NanoParticle doped EBF (NPEBR) at high and low doses, as reported in Fig. 13 – 14 and Fig 15 – 16. A straightforward comparison with the results of the EBF fiber (Al-doped) (cfr. Fig. 10 – 11) highlights a lower sensitivity, especially at high doses, but the same behavior (i.e., positive spectral shift at low dose and negative spectral shift at high dose) are observed. Unfortunately, this first NPEBF has so far exhibited lower detection capabilities, but it is expected that further engineering on the core doping (nanoparticles size and concentration) can improve its performance.

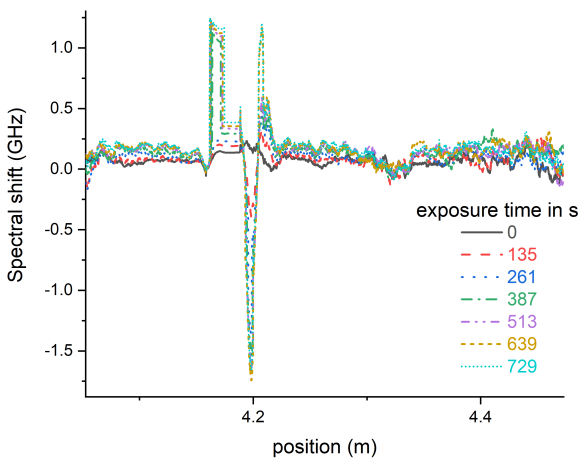

Fig. 13. Spectral shift versus position for the Mg nanoparticles-doped fiber (NPEBF) exposed at 710 Gy/min.

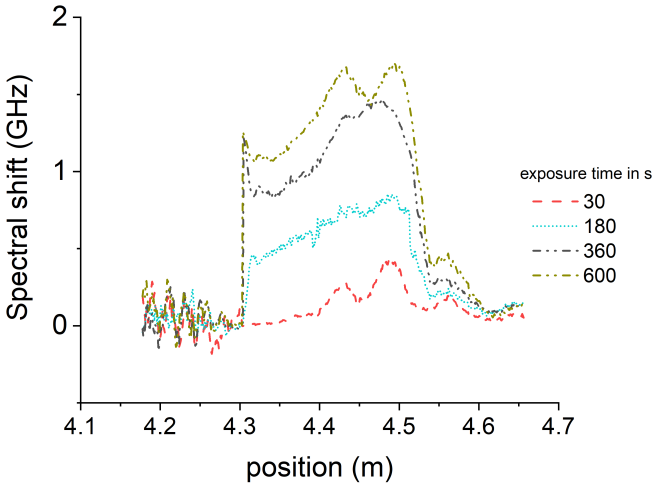

Fig. 15. Spectral shift along the NPEBF exposed at therapeutic dose of 2.2 Gy/min. It can be observed a positive trend, opposite to that observed at high doses (cfr. Fig. 13), just as it occurs for the Al-doped fiber.

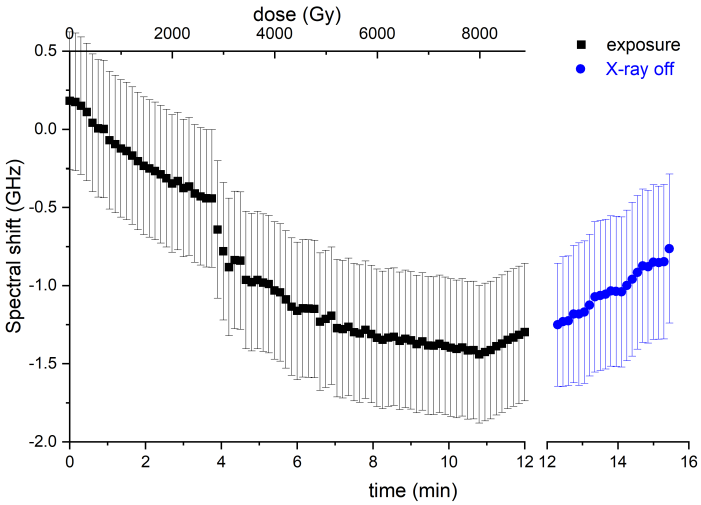

Fig. 14. Evolution of the spectral shift peak of the NPEBF fiber exposed at 710 Gy/min. The break of the horizontal axis is an artifact for more convenient reading.

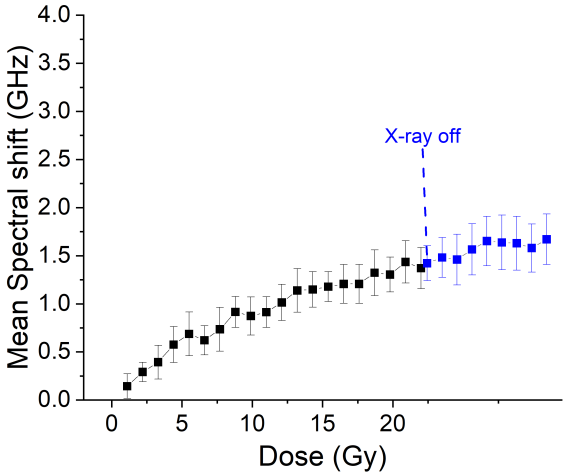

Fig. 16. Evolution of the spectral shift peak of the NPEBF exposed at 2.2 Gy/min.

C. Quasi-distributed FBG sensor

For this experiment a quasi-distributed sensor was fabricated in the NPEBF by writing a dense array of FBGs with a femtosecond laser using a technique similar to that described in Ref. [22] for SMFs. The FBGs had a length of 5 mm each, spaced by 2 mm. The response of the FBG array was recorded by a commercial high speed FBG interrogator (MicronOptics, model si255). Fig. 17 shows the spectral response of the FBG array. Unfortunately, the peak of the FBGs at 1541 nm and 1547 nm could be hardy detected by the peak tracking algorithm during the exposure experiments because of their lower reflectivity and therefore had to be excluded from the analysis for the too many artifacts. It is expected that the quality of the femto-written FBGs will improve as the NPEBF is optimized.

The real-time comparison between distributed and quasi-distributed sensing was made by exposing during the high dose experiment of the NPEBF fiber a twin sample with the FBG array. The Bragg wavelengths were recorded at 1 kHz and the data were smoothed by adjacent averaging of 1000 samples. Fig. 18 depicts the evolution of the Bragg peaks during exposure at 710 Gy/min. The gratings exhibit an absolute shift up to about 33 pm, that corresponds to a RIRIC in the order of 3×10^{-5}. Notice that both red and blue shifts of the Bragg peaks are observed, which further supports the hypothesis of two competing phenomena in the radiation-induced defects as it is observed when recording the spectral shift with the OBR. As expected, the acquisition rate with the FBG-based approach can be set much higher than that with the OBR/EBR system (kHz vs. Hz), but this occurs at the price of a reduced resolution and/or limited spatial range. Furthermore, an optical

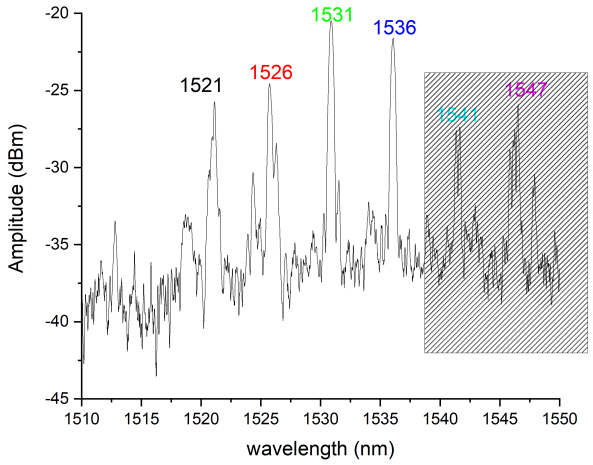

Fig. 17. Spectral response of the FBGs inscribed into the NPEBF by femtosecond direct laser writing. The FBGs at 1541 and 1547nm (in the gray-pattern frame) could not be tracked during the irradiation experiment.

fiber requires an extra fabrication step to be equipped with an FBG array, that may be inconvenient for disposable dosimetry sensors. These pros and cons shall be then further investigated in a real framework.

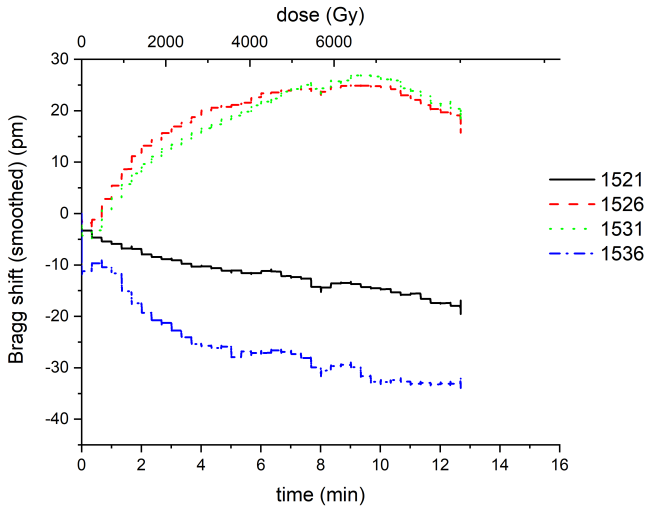

Fig. 18. Bragg shift of the FBGs inscribed into the NPEBF and exposed at $710\,\mathrm{Gy/min}$, during the same experiment of Fig 13 and Fig 14.

IV. Conclusions

A new setup for real-time distributed X-ray dosimetry based on fiber optics has been presented. The system exploits an enhanced backscattering optical fiber as the sensing element, interrogated with an optical backscatter reflectometer that can measure the local spectral shift of the Rayleigh scattering along the fiber. The measurements demonstrate a detection capability down to $2\,\mathrm{Gy/min}$ with a sub mm resolution. The enhanced backscattering optical fiber is based on an ad-hoc Aluminum-doped fiber. Further experiments have been carried out using a Magnesium nanoparticles-doped enhanced backscattering fiber in a preliminary version. The fibers were exposed from high ($700\,\mathrm{Gy/min}$) to low ($2\,\mathrm{Gy/min}$) dose rates, demonstrating that both types of fiber can be used as sensors, with the Aluminum-doped fiber exhibiting a higher sensitivity. The measurements also highlighted that there are two competing phenomena that induce the response to radiation, that shall be further investigated for the development of more sensitive optical fibers. The experimental research also highlighted that the optical backscatter reflectometer is likely the most suitable instrument to implement distributed dosimetry with optical fibers because: 1) along with the Radiation Induced Attenuation (RIA) it can measure the Radiation Induced Refractive Index Change (RIRIC), which is a more sensitive parameter to radiation 2) it performs measurements with high spatial resolution. A proof-of-concept comparison with a quasi distributed sensing system based on an array of fiber Bragg gratings was also performed, confirming the results and discussing pros and cons of the two optical fiber-based sensing techniques. The overall work demonstrates that real-time dosimetry can be implemented in conventional and advanced radiotherapy treatments with the proposed system. Further developments shall be focused on extensive measurements to investigate new optical fibers with possible further enhanced sensitivity, a deep investigation of the physical effects of radiation on these fibers, an optimization of the instrument settings according to the application requirements (sensitivity, spatial resolution, sampling rate). Last but not least, economical aspects (such as the use of the fiber sensor as a disposable probe, the cost of the back-scattering reflectometer) must be carefully considered when moving from a proof-of-concept research to biomedical applications. As a perspective, the system shall be tested in a real or simulated framework of radiotherapy treatment to better asses its advantages and limits.

References

[1] A. Micke, D. F. Lewis, X. Yu, “Multichannel film dosimetry with nonuniformity correction,” *Med. Phys.*, vol. 38, pp. 2523–2534, 2011.
[2] K. Pushpavanam, et al., “Determination of topographical radiation dose profiles using gel nanosensors,” *Science Advances*, vol. 5, 2019.
[3] A.L.Palmer, P. Di Pietro, S. Alobaidli, F. Issa, S. Doran, D. Bradley, A. Nisbet, “Comparison of methods for the measurement of radiation dose distributions in high dose rate (HDR) brachytherapy: Ge-doped optical fiber, EBT3 Gafchromic film, and PRESAGE® radiochromic plastic,” *Med Phys.*, vol. 40, 2013.
[4] M. A. S. Zaghloul et al., ”High Spatial Resolution Radiation Detection Using Distributed Fiber Sensing Technique,” in IEEE Transactions on Nuclear Science, vol. 64, no. 9, pp. 2569-2577, Sept. 2017.
[5] D. D. Francesca et al., ”Qualification and Calibration of Single-Mode Phosphosilicate Optical Fiber for Dosimetry at CERN,” in Journal of Lightwave Technology, vol. 37, no. 18, pp. 4643-4649, 15 Sept.15, 2019.
[6] Z. Ding, C. Wang, K. Liu, J. Jiang, D. Yang, G. Pan, Z. Pu, and T. Liu, “Distributed Optical Fiber Sensors Based on Optical Frequency Domain Reflectometry: A review,” Sensors, vol. 18, no. 4, p. 1072, Apr. 2018.
[7] M. Olivero et al., ”Preliminary investigation of radiation dose sensors based on aluminum-doped silicate optical fibers,” presented at the 15th Edition of IEEE International Symposium on Medical Measurements and Applications, virtual, June 1st-July 1st, 2020.
[8] OBR4600 manual, chapt. 8. Luna Inc. Roanoke, VA 24011. https://lunainc.com/product/sensing-solutions/obr-4600/
[9] B.J. Soller, D.K. Gifford, M.S. Wolfe, and M.E. Froggatt, “High resolution optical frequency domain reflectometry for characterization of components and assemblies,” *Opt. Expr.*, vol. 13, no. 2, pp. 666–674, 2005.

[10] M. Froggatt and J. Moore, "High-spatial-resolution distributed strain measurement in optical fiber with Rayleigh scatter," *Appl. Opt.*, vol. 37, pp. 1735–1740, 1998.

[11] L. Cognolato. Chemical Vapour Deposition for Optical Fibre Technology. Journal de Physique IVColloque, 1995, 05 (C5), pp.C5-975-C5-987. DOI: 10.1051/jphyscol:19955115.

[12] J. E. Townsend, S. B. Poole and D. N. Payne, "Solution-doping technique for fabrication of rare-earth-doped optical fibres," in Electronics Letters, vol. 23, no. 7, pp. 329-331, 26 March 1987, doi: 10.1049/el:19870244

[13] W. Blanc, I. Martin, H. Francois-Saint-Cyr, X. Bidault, S. Chaussedent, C. Hombourger, S. Lacomme, P. Le Coustumer, D.R. Neuville, D.J. Larson, T.J. Prosa, C. Guillermier, "Compositional changes at the early stages of nanoparticles growth in glasses," *The Journal of Physical Chemistry C*, vol. 123, pp. 29008–29014, 2019.

[14] W. Blanc, V. Mauroy, L. Nguyen, B.N. Shivakiran Bhaktha, P. Sebbah, B.P. Pal, and B. Dussardier, "Fabrication of rare earth-doped transparent glass ceramic optical fibers by modified chemical vapor deposition," *J. Am. Ceram. Soc.*, vol. 94, pp. 2315–2318, 2011.

[15] R. Kashyap, Fiber Bragg Gratings (Academic, 1999).

[16] S. Girard, A. Alessi, N. Richard, L. Martin-Samos, V. De Michele, L. Giacomazzi, S. Agnello, D. Di Francesca, A. Morana, "Overview of radiation induced point defects in silica-based optical fibers," Rev. Phys. vol. 4, p. 100032, 2019.

[17] A. Beisenova, A. Issatayeva, S. Sovetov, S. Korganbayev, M. Jelbuldina, Z. Ashikbayeva, W. Blanc, E. Schena, S. Sales, C. Molardi, and D. Tosi, "Multi-fiber distributed thermal profiling of minimally invasive thermal ablation with scattering-level multiplexing in MgO-doped fibers," Biomed. Opt. Express 10, pp. 1282-1296, 2019.

[18] J. Wilson et al. "Ultra-High Dose Rate (FLASH) Radiotherapy: Silver Bullet or Fool's Gold?." Frontiers in oncology vol. 9 1563. 17 Jan. 2020, doi:10.3389/fonc.2019.01563.

[19] K. J. Harrington, "Ultrahigh Dose-rate Radiotherapy: Next Steps for FLASH-RT," Clinical Cancer Research 25(1), 3–5, 2019.

[20] R. M. de Kruijff, "FLASH radiotherapy: ultra-high dose rates to spare healthy tissue," International Journal of Radiation Biology 96(4), 419–423, 2020.

[21] W. Blanc et al.,"Compositional changes at the early stages of nanoparticles growth in glasses," *The Journal of Physical Chemistry C*, vol. 123, pp. 29008–29014, 2019.

[22] A. Beccaria et al., "Temperature monitoring of tumor hyperthermal treatments with optical fibers: comparison of distributed and quasi-distributed techniques," Optical Fiber Technology 60, p. 102340, 2020.